

High Efficiency Radial-Junction Si Nanohole Solar Cells Formed by Self-Assembling High Aspect Ratio Plasma Etching

Hua-Min Li¹, Dae-Yeong Lee¹, Yeong-Dae Lim¹, Cheng Yang¹, Gang Zhang¹, HyunJin Kim², SeungNam Cha², Jong Min Kim², and Won Jong Yoo^{1,*}

¹ Department of Nano Science and Technology, SKKU Advanced Institute of Nano-Technology (SAINT), Sungkyunkwan University, Suwon 440-746, Korea, * Phone: 82-31-290-7468, Fax: 82-31-299-4119, Email: yoowj@skku.edu

² Frontier Research Laboratory, Samsung Advanced Institute of Technology, Yongin 449-712, Korea

Abstract

A drastic improvement in conversion efficiency was achieved from Si solar cells with radial-junction nanohole structure of a high aspect ratio of ~10 which is fabricated by self-assembling plasma etching. A conversion efficiency of 27.8 % was predicted based on an optimization of various structural parameters by numerical simulations, and a design principle for realizing high efficiency Si nanohole surface texture for photovoltaic devices was demonstrated.

Introduction

Recently, Si radial-junction structures, *e.g.*, Si nanowire (SiNW) (1),(2), Si nanopillar (SiNP) (3)-(5), Si nanorod (SiNR) (6) and Si nanohole (SiNH) (7)-(9) for photovoltaic (PV) applications have received significant attention due to their outstanding optical and electrical performance (5)-(11), such as (i) large junction area due to its three dimensional structure, (ii) low light reflection due to the density-graded surface (12), (iii) high light absorption due to the strong diffraction and scattering in the textured surface (11), (iv) long distance in the incident (vertical) direction for optimal light absorption and short distance in the orthogonal (horizontal) direction for effective minority-carrier collection (6), and (v) low-cost mass production via the use of low-grade Si raw materials (3),(4) *etc.*. However, the fabrication of those radial-junction structures so far requires high-cost processes, *e.g.*, vapor-liquid-solid (VLS) growth as the bottom-up method or lithography involved etching process as the top-down method *etc.* (7),(13), which are not only uneconomic but unpractical for the mass production. In this work, the radial-junction SiNH solar cells of a high aspect ratio of ~10 were fabricated by a plasma etching process which self-assembles light-trapping nano-structure surface textures without requiring any pattern masks. The radial-junction SiNH showed a clear improvement in conversion efficiency (η) compared to the radial-junction SiNW solar cells, and a maximum η of 27.8 % was predicted by numerical simulations. Furthermore, a design principle in terms of various structural parameters, *e.g.*, substrate thickness, height, junction depth, feature radius, periodicity and emitter doping concentration *etc.* was demonstrated for realizing high efficiency SiNH PV devices.

Device Fabrication

Firstly, the SiNH and SiNW surface textures were self-assembled on a pre-cleaned 200-um-thick *p*-type multicrystalline Si (mc-Si) wafer via a maskless etching process using an inductively coupled plasma (ICP) etcher. Chamber pressure and bias power were set constantly at 30 mTorr and 600 W, respectively. O₂/SF₆ ratio and etching time were

optimized experimentally, which were 1.80 and 150 s for the SiNW texture and as well as 2.24 and 500 s for the SiNH texture, respectively. After etching, the sample was cleaned in Piranha solution (H₂O₂:H₂SO₄=1:1) at 100 °C for 20 min and buffered HF (aqueous, HF:NH₄F=1:6) at the room temperature for 10 s in order to remove the organic residue and surface oxide layer. Next, an *n*⁺-*p* junction was formed by a spin-on dopant (SOD) process, activated by a rapid thermal annealing (RTA) at 900 °C for 30 s. Then, the sample surface was coated with an indium tin oxide (ITO) film via a RF sputtering to enhance the carrier collection, followed by the deposition of Ag and Al electrodes on the front and back surface, respectively, via a thermal evaporation. Finally, an annealing process in N₂ environment at 400 °C for 4 min was performed to form ohmic contact at metal-Si interface and to improve the transparency and conductivity of the ITO film.

Modeling and Simulaiton

Fig. 1 illustrates the schematic and energy band diagram of the SiNW and SiNH texture units. The radial-junction is divided into *n*-type quasi-neutral region (*n*-QNR), *p*-type quasi-neutral region (*p*-QNR) and depletion region for analysis. Firstly, the height (*H*)-dependent currents from *p*-QNR ($J_{p-QNR(\varepsilon)}$), *n*-QNR ($J_{n-QNR(\varepsilon)}$) and depletion region ($J_{dep(\varepsilon)}$) were obtained by solving the transport equations with their boundary conditions, in which both front and back surface recombination (S_f and S_b) were included (6). Then, the effective currents from *p*-QNR (J_{p-QNR}), *n*-QNR (J_{n-QNR}) and depletion region (J_{dep}) were calculated by integrating the *H*-dependent currents with their corresponding areas (6), as listed in Table 1. Finally, the effective current for the complete radial-junction ($J_{sum} = J_{p-QNR} + J_{n-QNR} + J_{dep}$) as a function of an applied voltage (V_{app}) was obtained, as shown in Fig. 2. Considering both the contributions from the planar- and radial-junctions, the maximum η of 27.8 % for the single SiNH structure is predicted, which is ~36.3 % higher compared to the single SiNW structure (η of 20.4 %) with the identical structural parameters, indicating an outstanding enhancement of the photocurrent generation in the SiNH structure. In addition, this drastic improvement is mainly contributed by the significant increase of J_{p-QNR} (see Fig. 2(c) and (d)) due to the relatively larger volume and higher minority-carrier concentration of *p*-QNR in the SiNH structure.

Results and Discussion

The high aspect ratio of ~10 in the SiNH and SiNW surface structures was observed by a scanning electron microscope (SEM) (see Fig. 1(b)). The nano-structure was self-assembled during the etching process, owing to (i) the surface roughness induced by the local surface oxidation, (ii)

the synergistic effects between surface oxidation and ion scattering, and (iii) the difference between vertical etching rates and sidewall etching rates in the nano-structure (14). Both their output performances were tested by a solar simulator. The SiNH device shows a higher η of ~17.5 % compared to the SiNW device (η of ~14.1 %) (see Fig. 2(e) and (f)) and this is consistent with our simulation results.

Furthermore, the output performance of the radial-junction in the SiNH structure is examined in terms of the following structural parameters, which provides a design principle for realizing high efficiency radial-junction SiNH solar cells.

(i) Substrate thickness (t). In the radial-junction, only J_{p-QNR} varies with t due to the t -dependent width of p -QNR which is defined as the region between the depletion layer and back electrode. As t increases from 2 um (the thin film devices) to 200 um (the wafer-based devices), J_{p-QNR} and thereby J_{sum} are increased due to the enhanced photon absorption in the extended p -QNR, giving rise to an increase of η , as shown in Fig. 3(a).

(ii) Height (H). The increase of H relatively extends p -QNR and enhances the photon absorption in the incident direction, resulting in an improved performance, as shown in Fig. 3(b). However, J_{sum} and η start to saturate as $H > 2$ um since 81.9 % of the photons are absorbed within 2 um in the exponential fashion. Therefore, ~2 um is considered as the optimized height for radial-junction structure.

(iii) Junction depth (x_n-x_n'). x_n-x_n' directly affects the width of n -QNR and the junction area ($A_j = 2\pi(d/2+x_n-x_n')H$). As it increases from 0.02 to 0.3 um, J_{n-QNR} is increased due to the enhanced photon absorption in the extended n -QNR. Meanwhile, the enlarged A_j leads to an enhancement in J_{dep} and J_{p-QNR} , resulting in an improvement in the photocurrent generation and η , though the extension of n -QNR degrades the carrier collection due to the increased transport distance, as shown in Fig. 3(c).

(iv) Feature radius ($d/2$) and periodicity (D). The increase of $d/2$ enlarges A_j and enhances the photocurrent generation for a single unit, but it also reduces the unit density and then the total photocurrent generation for a multi-unit system. Therefore, a D -dependent collecting area ($A_c = 0.25\pi D^2$) is used to present the array periodicity's effect. As $d/2$ increases for a constant D ($D = 4$ um), the d/D ratio is increased, indicating an enhanced contribution of the radial-junction in the SiNH structure compared to the planar-junction, and giving rise to an increase of J_{sum} and η . However, as $d/2$ increases for the constant d/D ratio ($d/D = 0.5$), the increase of D -dependent A_c is relatively larger than that of d -dependent A_j , resulting in a degraded performance (see Table 1), as shown in Fig. 4.

(v) Emitter doping concentration (N_D). The surface texture enhances the front surface recombination inevitably due to the relatively enlarged surface area, and consequently induces a degradation of η . Increasing N_D is one solution for suppressing the surface recombination due to the reduction of minority-carrier concentration (3),(4). However, the carrier collection is also reduced for high N_D due to the degradation of carrier mobility (μ_p), lifetime (τ_p), diffusion coefficient (D_p) and length (L_p) etc.. These parameters and N_D synthetically affect the complete electrical performance of the SiNH solar cell, as shown in Fig. 5. As a result of trade-off

between these two competing mechanisms, when N_D increases from 10^{17} to 10^{22} cm $^{-3}$, short-circuit J_{sum} ($J_{sum,SC}$) shows a peak at N_D of 10^{20} cm $^{-3}$ where open-circuit voltage (V_{oc}) is maintained steadily, giving rise to a maximized η even S_f is on the order of 10^6 cm/s. This indicates 10^{20} cm $^{-3}$ as an optimized N_D for the SiNH solar cells.

In summary, the radial-junction SiNH solar cell shows a better performance compared to the other types of surface textured solar cells, e.g., planar cell (6), pyramidal cell (15),(16), Si nanocone (SiNC) (3) and SiNW (3),(5),(6) etc., as listed in Table 2.

Conclusion

In this paper, the drastic improvement in the conversion efficiency of Si nanohole solar cells compared to the Si nanowire solar cells was demonstrated by the simulation and confirmed by the experiments. The Si nanohole and nanowire surface structures with the high aspect ratio were self-assembled by the maskless plasma etching process. The maximum efficiency of 27.8 % from Si nanohole solar cells was predicted by optimizing various structural parameters.

References

- (1) B. Tian, X. Zhang, T. J. Kempa, Y. Fang, N. Yu, G. Yu, J. Huang, and C. M. Lieber, "Coaxial silicon nanowires as solar cells and nanoelectronic power sources," *Nature*, vol. 449, no. 7146, pp. 885-889, Oct 2007.
- (2) Z. W. Pei, S. T. Chang, C. W. Liu, and Y. C. Chen, "Numerical simulation on the photovoltaic behavior of an amorphous-silicon nanowire-array solar cell," *IEEE Electron Device Lett.*, vol. 30, no. 12, pp. 1305-1307, Dec. 2009.
- (3) J. S. Li, H. Y. Yu, S. M. Wong, G. Zhang, X. W. Sun, G. Q. Lo, and D. L. Kwong, "Surface nanostructure optimization for solar energy harvesting in Si thin film based solar cells," in *IEDM Tech. Dig.*, 2009, pp. 547-550.
- (4) S. M. Wong, H. Y. Yu, J. S. Li, G. Zhang, P. G. Q. Lo, and D. L. Kwong, "Design high-efficiency Si nanopillar-array-textured thin-film solar cell," *IEEE Electron Device Lett.*, vol. 31, no. 4, pp. 335-337, Apr. 2010.
- (5) J. S. Li, H. Y. Yu, S. M. Wong, G. Zhang, X. W. Sun, P. G. Q. Lo, and D. L. Kwong, "Si nanopillar array optimization on Si thin films for solar energy harvesting," *Appl. Phys. Lett.*, vol. 95, no. 3, 033102, Jul. 2009.
- (6) B. M. Kayes, H. A. Atwater, and N. S. Lewis, "Comparison of the device physics properties of planar and radial p-n junction nanorod solar cells," *J. Appl. Phys.*, vol. 97, no. 11, 114302, May 2005.
- (7) K.-Q. Peng, X. Wang, L. Li, X.-L. Wu, and S.-T. Lee, "High-Performance Silicon Nanohole Solar Cells," *J. Am. Chem. Soc.*, vol. 132, no. 20, pp. 6872-6873, Apr. 2010.
- (8) S. E. Han and G. Chen, "Optical Absorption Enhancement in Silicon Nanohole Arrays for Solar Photovoltaics," *Nano Lett.*, vol. 10, pp. 1012-1015, Feb. 2010.
- (9) F. Wang, H. Y. Yu, J. S. Li, X. W. Sun, X. C. Wang, and H. Y. Zheng, "Optical absorption enhancement in nanopore textured-silicon thin film for photovoltaic application," *Opt. Lett.*, vol. 35, no. 1, Jan. 2010.
- (10) M. D. Kelzenberg, D. B. Turner-Evans, B. M. Kayes, M. A. Filler, M. C. Putnam, N. S. Lewis, and H. A. Atwater, "Photovoltaic measurements in single-nanowire silicon solar cells," *Nano Lett.*, vol. 8, no. 2, pp. 710-714, Feb. 2008.
- (11) R. A. Street, P. Qi, R. Lujan, and W. S. Wong, "Reflectivity of disordered silicon nanowires," *Appl. Phys. Lett.*, vol. 93, no. 16, 163109, Oct. 2008.
- (12) H. C. Yuan, V. E. Yost, M. R. Page, P. Stradins, D. L. Meier, and H. M. Branz, "Efficient black silicon solar cell with a density-graded nanoporous surface: optical properties, performance limitations, and design rules," *Appl. Phys. Lett.*, vol. 95, no. 12, 123501, Sep. 2009.
- (13) K.-Q. Peng and S.-T. Lee, "Silicon Nanowires for Photovoltaic Solar Energy Conversion," *Adv. Mater.*, vol. 23, pp. 198-215, Oct. 2010.
- (14) H. Tsuda, M. Mori, Y. Takao, K. Eriguchi, and K. Ono, "Atomic-scale cellular model and profile simulation of Si etching: Formation of surface roughness and residue," *Thin Solid Film*, vol. 518, pp. 3475-3480, Nov. 2009.
- (15) J. C. Zolper, S. Narayanan, S. R. Wenham, and M. A. Green, "16.7% efficient, laser textured, buried contact polycrystalline silicon solar cell," *Appl. Phys. Lett.*, vol. 55, pp. 2363-2365, Nov. 1989.
- (16) J. Zhao, A. Wang, P. Altermatt, and M. A. Green, "Twenty-four percent efficient silicon solar cells with double layer antireflection coatings and reduced resistance loss," *Appl. Phys. Lett.*, vol. 66, pp. 3636-3638, Jun. 1995.

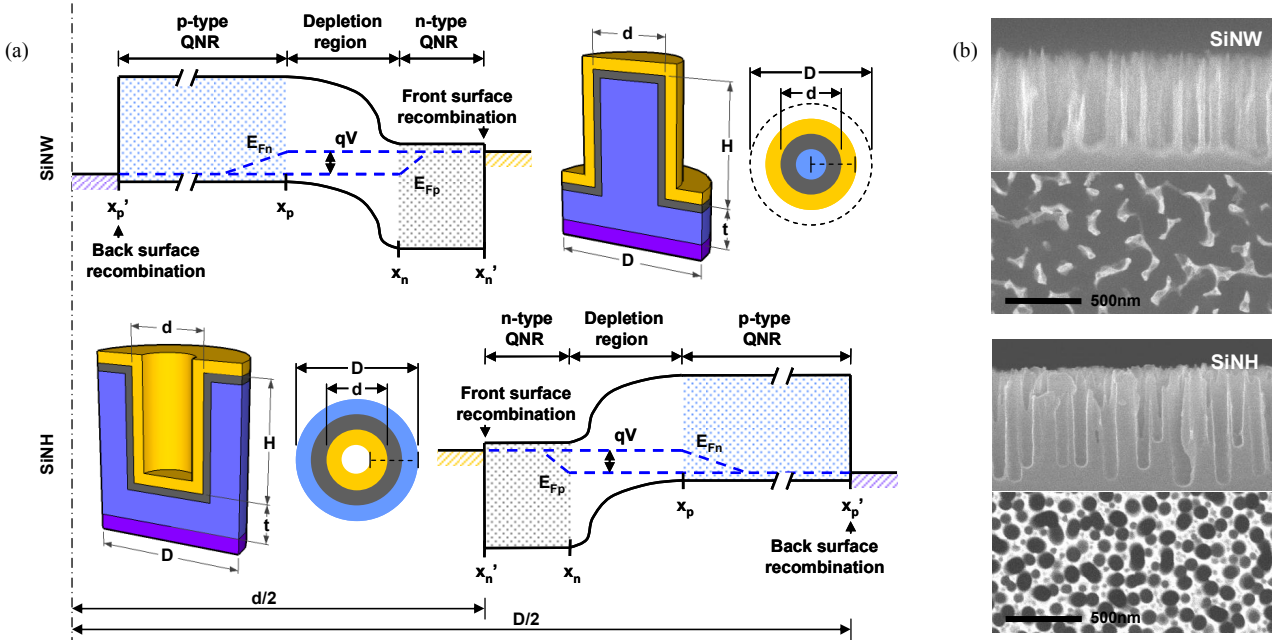


Fig. 1. (a) Schematic and energy band diagram of single radial-junction SiNW and SiNH structures. p -QNR ($x_p < x < x_p'$), n -QNR ($x_n' < x < x_n$) and depletion region ($x_n < x < x_p$) of the radial-junction as well as the front and back surface recombination are illustrated. d , D , H and t are feature diameter, periodicity, height and substrate thickness, respectively. (b) SEM images of the SiNW and SiNH surface structures. The high aspect ratio of ~10 was observed.

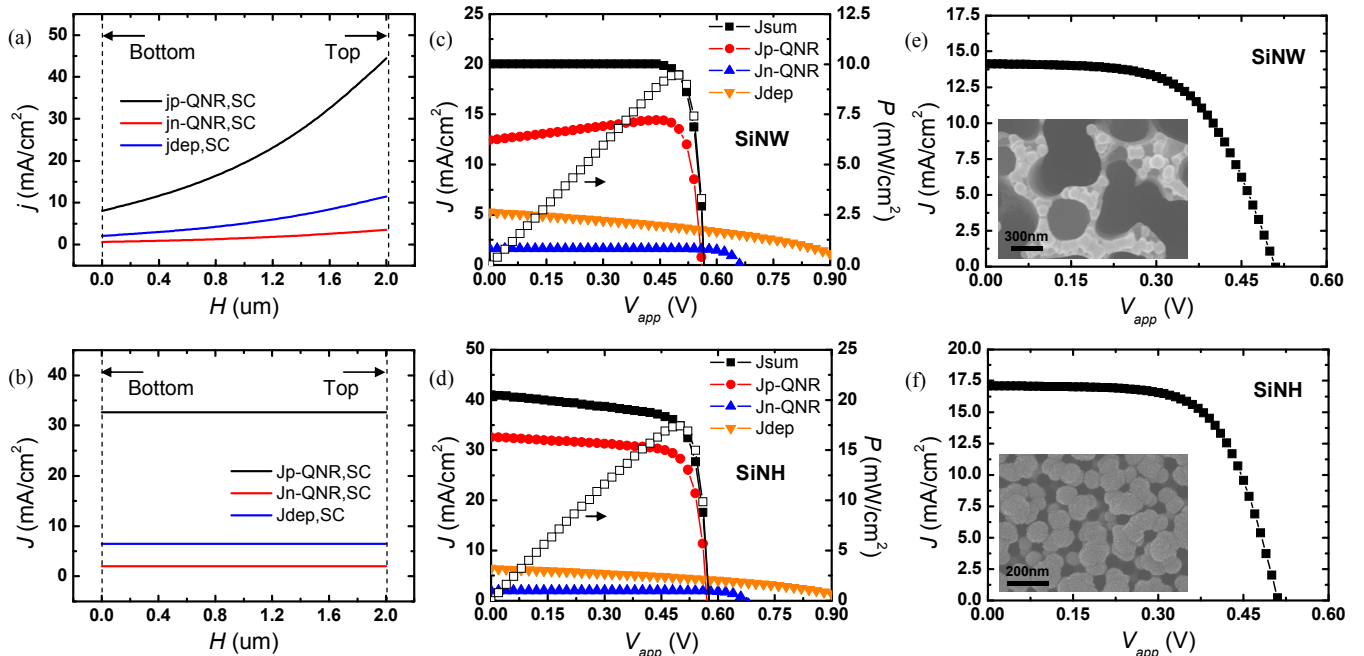


Fig. 2. (a) H -dependent short-circuit current density ($j_{p-QNR,SC}$, $j_{n-QNR,SC}$ and $j_{dep,SC}$) in the radial-junction, which is lowered at the bottom due to the exponential reduction of photon flux. (b) Effective short-circuit current density ($J_{p-QNR,SC}$, $J_{n-QNR,SC}$ and $J_{dep,SC}$) obtained by integrating the H - dependent current density with the corresponding areas. (c) J_{sum} (including J_{p-QNR} , J_{n-QNR} and J_{dep}) and P as functions of V_{app} in the radial-junction for the SiNW structure and (d) for the SiNH structure. Considering the contributions from both the planar-junction (η of 10.9 %) and the radial-junction (η of 17.4 %) of SiNH structure, a total conversion efficiency of 27.8 % is obtained, when $d=2\text{ }\mu\text{m}$, $H=2\text{ }\mu\text{m}$, $t=200\text{ }\mu\text{m}$, $D=4\text{ }\mu\text{m}$, $x_n-x_p'=0.1\text{ }\mu\text{m}$, base doping concentration ($N_A=10^{16}\text{ cm}^{-3}$, $N_D=10^{20}\text{ cm}^{-3}$, $S_f=S_b=10^4\text{ cm/s}$). (e) Experimental results of the SiNW and (f) the SiNH solar cells with the SEM images of their surfaces.

Table 1. Formulas for H -dependent current density j and effective current density J used in SiNH simulations.¹

p -QNR	n -QNR	Depletion region
$j_{p-QNR}(z) = -qD_n \frac{dn_p}{dx} \Big _{x=x_p}$	$j_{n-QNR}(z) = qD_p \frac{dp_n}{dx} \Big _{x=x_n}$	$j_{dep}(z) = q\Gamma(z)\{1 - \exp[-\alpha(x_p - x_n)]\}$
$J_{p-QNR} = \frac{2\pi x_p \int_0^H j_{p-QNR}(z) dz}{0.25\pi D^2}$	$J_{n-QNR} = \frac{2\pi x_n \int_0^H j_{n-QNR}(z) dz}{0.25\pi D^2}$	$J_{dep} = \frac{2\pi \left(x_p - \frac{1}{2}W_{dep} \right) \int_0^H j_{dep}(z) dz}{0.25\pi D^2}$

¹ $n_p(p_p)$, $n_{p0}(p_{n0})$ and $D_n(D_p)$ are nonequilibrium and equilibrium density, diffusion coefficient for the minority-carrier of electrons (holes) in p -QNR (n -QNR), respectively. q is the electronic charge. α is the absorption coefficient of Si. Γ is the photon flux of AM1.5 spectrum. W_{dep} is the depletion width.

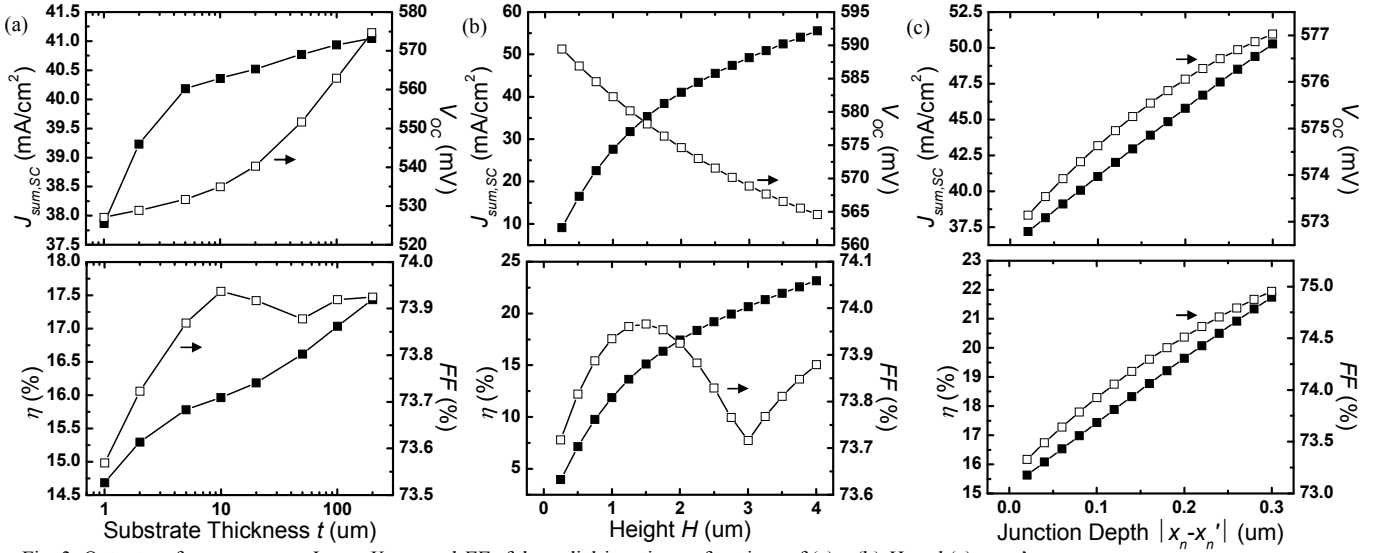


Fig. 3. Output performance, e.g., $J_{sum,SC}$, V_{OC} , η and FF of the radial-junction as functions of (a) t , (b) H , and (c) $x_n - x_n'$.

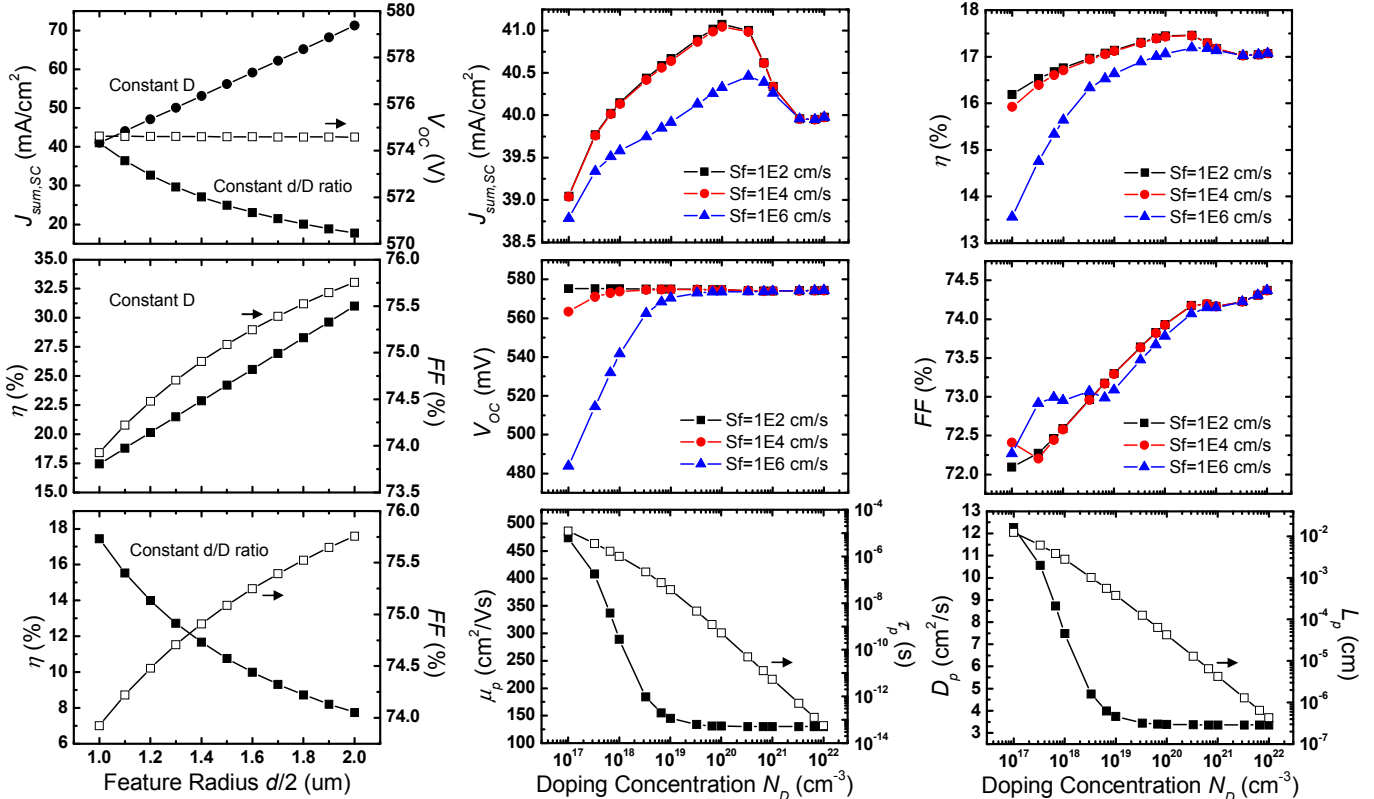


Fig. 4. Output performance of the radial-junction as a function of $d/2$. Constant D and d/D ratio indicate the enhanced and reduced contribution of the radial-junction in the SiNH structure, respectively.

Fig. 5. Output performance of the radial-junction and the physical properties of the minority carrier in n -QNR, e.g., μ_p , D_p and L_p as functions of N_D for various S_f levels. The peaks of $J_{sum,SC}$ and η at 10^{20} cm^{-3} indicate an optimized N_D for the SiNH structure, resulting from a trade-off between the suppressed front surface recombination and the degraded carrier collection.

Table 2. Comparison of the performance between radial-junction SiNH and the other types of textured solar cells.

Types Parameter \	This work: SiNH (radial-junc.)	Si planar cell (6)	Si pyramidal cell (15) (upright) ¹	Si pyramidal cell (16) (inverted) ¹	Si nanocone (SiNC) (3)	SiNW (5) (subsurface-junc.)	SiNW (3) (planar-junc.)	SiNW (6) (radial-junc.)
Schematic of single unit								
J_{SC} (mA/cm 2)	66.6	~35	36.9	40.9	/	/	/	~43
V_{OC} (V)	0.56	~0.6	0.60	0.71	/	/	/	~0.52
η (%)	27.8	~18	16.7	24.0	~22.5	~27	~17.5	~17
FF (%)	74.6	/	75.2	82.7	/	/	/	/

¹ Those results were obtained via the experiments in which various techniques, e.g., antireflection coating and buried top contact etc. were also included.